High-pressure dielectric and lattice vibration studies of the phase transition in lithium thallium tartrate monohydrate (LTT)

1996 J. Phys.: Condens. Matter 8 4631

(http://iopscience.iop.org/0953-8984/8/25/018)

J. Phys.: Condens. Matter **8** (1996) 4631–4642. Printed in the UK

High-pressure dielectric and lattice vibration studies of the phase transition in lithium thallium tartrate monohydrate (LTT)

S Kamba†‡, G Schaack‡, J Petzelt† and B Březina†

† Institute of Physics, Czech Academy of Science, Na Slovance 2, 180 40 Prague 8, Czech Republic

‡ Physikalisches Institut der Universität Würzburg, Am Hubland, D–97074 Würzburg, Germany

Received 19 February 1996, in final form 24 April 1996

Abstract. A substantial increase of the ferroelectric phase transition temperature with hydrostatic pressure was observed for lithium thallium tartrate monohydrate single crystals. The temperature dependence of the permittivity ε'_a shows an unusual shape exhibiting a broad plateau in $\varepsilon'_a(T)$ below T_c. It follows from our hysteresis loop measurements that the domain wall motion freezes approximately 5–15 K (this value is pressure dependent) below T_c and causes the drop in $\varepsilon'_a(T)$. The temperature and pressure dependence of the soft-mode frequency was measured by far-infrared as well as Raman spectroscopy at 10–300 K and 0.1–440 MPa. The soft mode softens only incompletely because of its strong coupling with a transverse acoustic mode.

1. Introduction

Lithium thallium tartrate monohydrate (LTT)—$LiTlC_4H_4O_6 \cdot H_2O$—undergoes at $T_c = 11$ K a second-order phase transition (PT) from the paraelectric (PE) (space group $P2_12_12$ (D_2^3) ($Z = 4$) [1, 2]) to a ferroelectric (FE) phase of unknown symmetry [3, 4, 5, 6]. The free permittivity $\varepsilon'_a(T)$ along the a-axis shows a large value ($\sim$5000) near T_c. $\varepsilon'_a(T)$ obeys the Curie–Weiss law very well above T_c, but below T_c, $\varepsilon'_a(T)$ does not vary much—only a slight decreasing tendency is seen down to liquid helium temperature [3, 4, 5, 6] in contrast to the behaviour of usual ferroelectrics, whose permittivity falls steeply below T_c. Fousek *et al* explained the high value of the permittivity below T_c by the contribution of domain wall motion [4]. Sawaguchi and Cross have observed [7] that the permittivity is very sensitive to the mechanical boundary conditions. The free dielectric constant $\varepsilon'_a(T_c)$ reaches $\sim 5 \times 10^3$, whereas the clamped $\varepsilon'_a(T_c)$ is only $\sim$30. Both the elastic compliance at constant electric field s_{44}^E and the piezoelectric coefficient d_{14} become exceedingly large close to T_c and appear to have the highest magnitude measured in any material [7].

Gerbaux *et al* observed a soft mode (SM) in far-infrared (FIR) spectra and concluded that the PT in LTT is displacive [8]. Volkov *et al* measured the SM more carefully and found that its frequency softens from 21 cm^{-1} (at 300 K) to 9 cm^{-1} (at T_c) only and the dielectric contribution of this mode is one or two orders of magnitude smaller than the observed permittivity near T_c at low frequencies [9]. Therefore they concluded that the observed mode is not responsible for the phase transition in LTT and that another dispersion of the relaxational type should exist in the microwave region. In this case the

0953-8984/96/254631+12$19.50

PT should not be purely displacive but of mixed displacive–order–disorder type. Dielectric measurements [7, 10] revealed huge piezoelectric resonances in the range 10^4–10^6 Hz and the high-frequency permittivity corresponds very well to $\varepsilon'_a(T)$ in the submillimetre region. No relaxation-type absorption exists in the microwave range and the complete anomaly in the clamped permittivity $\varepsilon'_a(T_c)$ near T_c can be explained by the SM contribution. The incomplete softening of the SM is caused by its giant coupling with a transverse acoustic mode [10]. The PT in LTT is due to the soft polar phonon near 20 cm^{-1}; therefore the PT is displacive. No anomaly was found in the elastic stiffness for constant electric displacement; therefore the PT is regarded as a proper ferroelectric one [10]. This is in contrast to the case of isomorphous lithium ammonium tartrate monohydrate, which reveals a proper ferroelastic PT.

The SM has the symmetry B_3 in the paraelectric phase; therefore it should be both IR (for the electric field $\boldsymbol{E}\|\boldsymbol{a}$) and Raman active (in $\boldsymbol{bc}$ spectra). It was actually observed in Raman spectra by Khaller *et al* [11], but in contrast to the near-millimetre data [9] they have found softening of the SM to 15 cm^{-1} only, no hardening of this mode was observed below T_c (down to 2 K) and no new modes appeared in Raman spectra below T_c. Khaller *et al* concluded that the symmetry of the unit cell remained unchanged below T_c and that only the orientation of OH groups is responsible for the occurrence of P_s.

The aim of this paper is to study in more detail the temperature dependences of FIR and Raman spectra in an effort to understand the mechanism of the PT. Special care is devoted to dielectric and lattice vibration properties of LTT under high hydrostatic pressure.

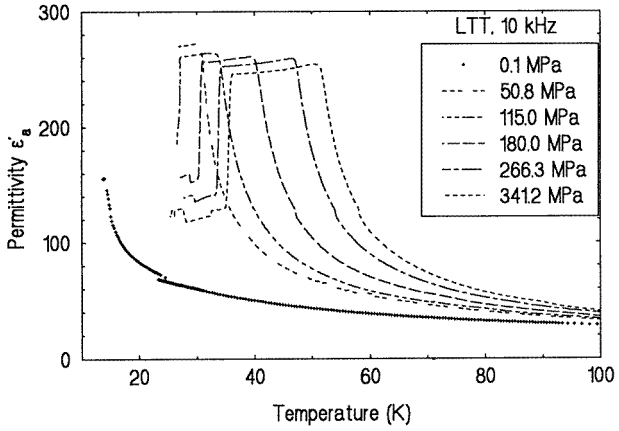

Figure 1. Temperature dependences of the permittivity ε'_a of LTT ($\boldsymbol{E}\|\boldsymbol{a}$, $dT/dt < 0$) at ambient and elevated hydrostatic pressures. All of the curves were obtained at 10 kHz. The small discontinuity near 25 K is an artefact of the instrument.

2. Experimental procedure

A LTT single crystal with a volume of several cm^3 was grown from aqueous solution [5]. For the dielectric and IR measurements, samples of plate shape (diameter 5–10 mm, thickness 0.2–1 mm) with orientation perpendicular to all crystallographic axes were cut from the single crystal. The sample for Raman scattering was of rectangular shape $\sim 4 \times 3 \times 6$ mm^3. All of the samples were oriented with polarized light and optically polished. For dielectric measurements circular aluminium electrodes evaporated at high vacuum were used. Both

the ε'- and ε''-parts of the complex dielectric function $\varepsilon^* = \varepsilon' + \mathrm{i}\varepsilon''$ were measured in the temperature region 20–300 K at hydrostatic pressures 0.1–400 MPa, using a Wayne–Kerr B905 A or a Keithley 3322 automatic bridge operating under computer control alternatively at frequencies $f = 0.1$, 0.4, 1, 10 kHz and $f = 0.5$, 1, 5, 10, 50 and 100 kHz, respectively. The measuring field was 3 V cm^{-1} (Wayne–Kerr) or 16 V cm^{-1} (Keithley). Low temperatures were achieved in a liquid helium evaporation cryostat and the temperature drifts were controlled automatically (the drifts $|\mathrm{d}T/\mathrm{d}t|$ were 5 K h^{-1} $\leqslant |\mathrm{d}T/\mathrm{d}t| \leqslant$ 15 K h^{-1}).

Table 1. Phonon mode frequencies in LTT at 70 K (the paraelectric phase) observed in Raman and IR spectra. A, B_1, B_2 and B_3 specify the symmetry of phonon modes and δ, β and τ represent the angles of deformation, bond bending and torsion, respectively, of the indicated group.

A	B_3		B_2		B_1		
$b(aa)c$	$b(cb)c$	$\boldsymbol{E}\|\boldsymbol{a}$	$b(ca)c$	$\boldsymbol{E}\|\boldsymbol{b}$	$b(ab)c$	$\boldsymbol{E}\|\boldsymbol{c}$	Assignment
	13.5	14.3					
30.3		32.3		27.6			
39.6	38.5	39.4				33.5	
	50.2	48.9	51.1	49.8	51.1		
64.0	56.0	55.9	63.1	62.7	63.5	63.0	
	70.4	69.5		70.8	71.6		$\beta_{C(OH)}$
					77.0		δ_{CCC}
83.3	83.0	85.0	86.4			85.7	CC twist
	91.5	90.4		91.1	94.0		and external
	101.4	101.2	101.4	104.5		102.5	lattice modes
121.6	122.5	121.5	123.1	122.8			
140.0		131.6	136.7	143.1	136.1		
157.5	159.7	159.0	157.9	156.0	157.6		
177.5	173.1	172.9	172.7				
186.5				184.2			
202.0		190.0	205.0	203.7			
	227.0	226.5	234.0		215.6		
265.8	254.0	252.6	254.2				δ_{CCC}
281.0	281.2	281.6		278.6	281.3		$\delta_{C(OH)}$
		296.4		292.1			
352.6		352.9		352.9			
377.7		376.9	377.6				$\beta_{C(OH)}$
415.3		432.6	415.3	419.1			
489.1	490.0	487.8	490.5		490.0		
			501.0				δ_{COO}
			523.8				τ_{COO}
			537.0				
546.0		540.5	546.0				
639.7	628.4		592.4				

FIR spectra were taken using a Grubb–Parsons Fourier spectrometer at hydrostatic pressure from 0.1 to 380 MPa with helium gas as the pressure-transmitting medium.

Raman scattering spectra were obtained using a Dilor XY spectrometer equipped with a liquid-nitrogen-cooled CCD detector. An argon laser with $\lambda = 514.5$ nm was used as the excitation source; the power of the beam at the sample was 100–200 mW. All of the spectra were taken in a 90° scattering geometry in the range 5–700 cm^{-1} at hydrostatic pressures up to 440 MPa. A resolution of 2.5 cm^{-1} in the spectra was achieved.

3. Experimental results and discussion

3.1. Dielectric measurements

The temperature dependences of the permittivity ε'_a at six different hydrostatic pressures are shown in figure 1. At ambient pressure (0.1 MPa) $\varepsilon'_a(T)$ was measured down to 15 K only; therefore the PT ($T_c = 11$ K) is not seen. The measured value of ε'_a is partially clamped due to the circular shape of the electrodes; therefore its value is one order of magnitude lower than the free permittivity and one order of magnitude higher than the clamped permittivity [7].

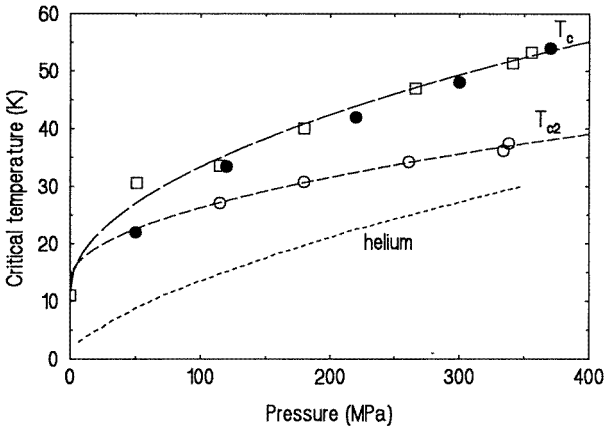

Figure 2. The pressure dependence of the FE PT temperature T_c obtained from independent dielectric (□ □ □) and Raman (● ● ●) experiments. T_{c2} signifies the temperature of the steep drop in $\varepsilon'_a(T)$ below T_c (the domain wall freezing temperature). The lowest dotted curve is the melting curve of ^{4}He [16].

Dielectric measurements at high hydrostatic pressure were performed only above 22 K. At high temperatures, $\varepsilon'_a(T)$ obeys the Curie–Weiss law very well and the extrapolated T_c lies systematically 5–6 K below the high-temperature peak in $\varepsilon'_a(T)$. However, in the following we shall consider this peak as the FE PT temperature (T_c) because near this temperature the SM frequency is minimum (see below). The increase of T_c with increasing pressure is clearly seen in figure 1 and shown in figure 2. An unusual plateau in $\varepsilon'_a(T)$ appears below T_c. Its width increases with pressure from ∼5 K (at 50 MPa) to ∼15 K (340 MPa). At a lower temperature, T_{c2}, ε'_a steeply drops down to half of its previous value. All of the curves in figure 1 were measured on cooling, but they are reproducible on heating with a small (2–3 K) thermal hysteresis of T_{c2}. The value of ε'_a is frequency independent below 10 kHz; at higher frequencies and temperatures between T_{c2} and T_c, ε'_a increases due to approaching piezoelectric resonances [7, 10], but the temperatures of the anomalies remain frequency independent. Like at ambient pressure in [6], two maxima in the dielectric loss $\varepsilon''_a(T)$ appear. The first one (near T_c) is frequency dependent and increases with increasing frequency. Our measured frequency range is too narrow to allow distinguishing of an Arrhenius from a Vogel–Fulcher behaviour. The second maximum at T_{c2} is frequency independent. Two samples of LTT with different thicknesses (600 and 190 μm) cut from one single crystal were used for dielectric measurements. The results obtained on the thicker sample are shown in figure 1. The thinner one has a similar shape

of $\varepsilon'_a(T, p)$ to that in figure 1, only the maximum at T_c is smoother, and $\varepsilon''_a(T)$ exhibits a plateau between T_{c2} and T_c without any peaks. A similar shape of $\varepsilon''_a(T)$ was observed by Fousek *et al* [4]. Both results show the importance of the boundary conditions of the sample (the thickness and the shape of the electrodes) for dielectric properties (the influence of piezoelectric resonances and domain wall mobility).

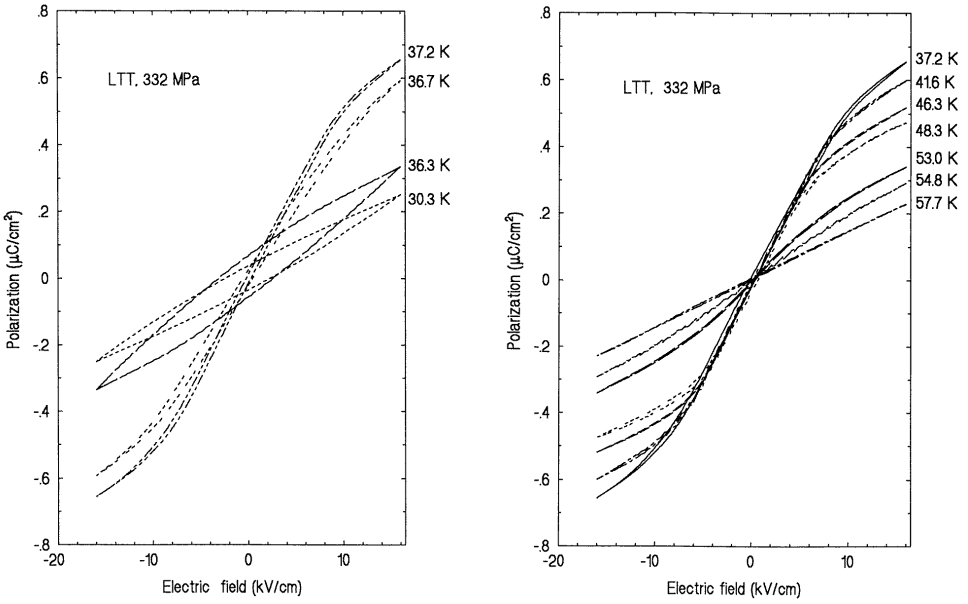

Figure 3. The temperature dependences of the hysteresis loops at 332 MPa. An electric field with a frequency of 10 Hz was applied along the FE *a*-axis.

What is the origin of the plateau in $\varepsilon'_a(T)$? A similar plateau (without a drop) was observed in the already published dielectric data for LTT [3, 4, 7] at ambient pressure. On the basis of dielectric measurements in bias fields, Fousek assigned it to a contribution from domain wall motions [4]. A similar shape of $\varepsilon'_a(T)$ with the plateau below T_c was also observed for KDP [12] and CsD_2AsO_4 crystals [14, 15]. The broad bump in the permittivity below T_c and the following slow drop on cooling were interpreted as a domain freezing out [13, 14, 15]. In our case, the drop in ε'_a at T_{c2} is very sharp. It might seem that this is connected with the mechanical clamping of the sample due to the solidification of helium in the pressure cell. However, helium solidifies $\sim$10 K below T_{c2} (see figure 2); therefore this effect is excluded. Another possible explanation of this drop is the existence of an additional structural PT in LTT. Several small drops in $\varepsilon'_a(T)$ appear also at high pressures and low temperatures, 20–30 K (see figure 1) below the large drop. Therefore the existence of another PT is not excluded, but the inhomogeneous freezing of ferroelectric domains or the inhomogeneous clamping of the sample is more probable. However, the structural analysis has been performed neither at low temperatures nor at high pressure.

The idea of a domain freezing out at T_{c2} is supported also by our hysteresis loop measurements of LTT (see figure 3). The ferroelectric hysteresis loops are extremely narrow (the coercive field E_c is less than 100 V cm^{-1}) in the temperature range of the plateau, but just below T_{c2} the loops widen considerably (see a huge change in the shape of the hysteresis loops between 36.7 K and 36.3 K in figure 3 (left panel); the temperature T_{c2}

lies between these values). It is impossible to switch the sample polarization below T_{c2} even with 16 kV cm^{-1} because of a freezing of domain walls. The loops with a small coercive field of 120 V cm^{-1} were reported at ambient pressure already in [3, 4]. Abe *et al* [6] observed two kinds of hysteresis loop for the same sample of LTT at the same temperature and ambient pressure; one had a very small (non-measurable) E_c and the other was open with $E_c = 240$ V cm^{-1}. The hysteresis loop with the small E_c appeared with a time delay of one month after the first measurement in which the open hysteresis loop ($E_c = 240$ V cm^{-1}) was observed. This suggests that the narrow hysteresis loop is more stable than the open one [6]. Abe *et al* concluded that the large electromechanical coupling in LTT might have an important role in the polarization-reversal process [6].

All of our hysteresis loops in figure 3 were taken at the relatively high frequency of 10 Hz. Loops observed at 1 and 0.1 Hz were more noisy. However, all of the loops were weakly opened. Also lossy dielectrics may have similar shape, but they have no anomaly in $\varepsilon'_a(T)$. Owing to a similarity with ferroelectric hysteresis loop measurements at ambient pressure [3, 4], we conclude that the sample is ferroelectric also at high pressure.

3.2. The infrared and Raman experiment

Raman and IR spectroscopy give important information about the crystal symmetry, because lattice vibration modes of different symmetry are seen in different kinds of spectra. A factor-group analysis and the selection rules for all lattice vibrations in the paraelectric phase of LTT yields

$$\Gamma_{LTT} = 56\mathrm{A}(\boldsymbol{a}^2, \boldsymbol{b}^2, \boldsymbol{c}^2) + 55\mathrm{B}_1(\boldsymbol{c}, \boldsymbol{ab}) + 57\mathrm{B}_2(\boldsymbol{b}, \boldsymbol{ac}) + 57\mathrm{B}_3(\boldsymbol{a}, \boldsymbol{bc}) + (\mathrm{B}_1 + \mathrm{B}_2 + \mathrm{B}_3)_{acoustic}. \quad (1)$$

The A modes are only Raman active while the B_1, B_2 and B_3 modes are both IR and Raman active. $\boldsymbol{a}$, $\boldsymbol{b}$, $\boldsymbol{c}$ indicate the polarization of the IR radiation parallel to the orthorhombic lattice vector and $\boldsymbol{a}^2$, $\boldsymbol{b}^2$, $\boldsymbol{c}^2$, $\boldsymbol{ab}$, $\boldsymbol{ac}$ and $\boldsymbol{bc}$ signify the elements of the symmetric Raman tensor. Considering tartrate and water molecules like rigid units, we can specify low-frequency external modes from (1) (without acoustic modes):

$$\Gamma_{LTTexternal} = 17\mathrm{A} + 16\mathrm{B}_1 + 18\mathrm{B}_2 + 18\mathrm{B}_3. \quad (2)$$

The other modes are internal vibrations of the tartrate and water groups.

Our measurements were performed only below 700 cm^{-1} where all external and part of the internal modes lie. Many modes were observed in all of the spectra. As an example, IR reflection spectra with polarization of the beam parallel to the polar axis $\boldsymbol{a}$ ($\boldsymbol{E}\|\boldsymbol{a}$) are shown in figure 4. The damping of all of the modes decreases on cooling; therefore 'new' modes appear in the spectra at low temperatures although no change of crystal symmetry occurs. The IR reflectivity and transmissivity were measured for all polarizations except for $\boldsymbol{E}\|\boldsymbol{c}$, where only transmission spectra were taken. The transmission experiment was performed only below 110 cm^{-1} due to growing opacity of the samples at high frequencies. All phonon modes observed in Raman and IR spectra of the paraelectric phase are summarized in table 1. The phonon frequencies were obtained from the fit of the IR spectra with the classical three-parameter oscillator model. The assignment of all of the modes is based on a similar mode analysis for Rochelle salt [17, 18].

Our IR and Raman spectra at ambient pressure were obtained only above T_c. The change of the crystal symmetry below T_c is clearly seen in the FIR spectra at high hydrostatic pressure. The most dramatic changes are seen in the range 80–110 cm^{-1} (see figure 5), where new modes appear in the FE phase at 84 and 98 cm^{-1} and the absorption band at

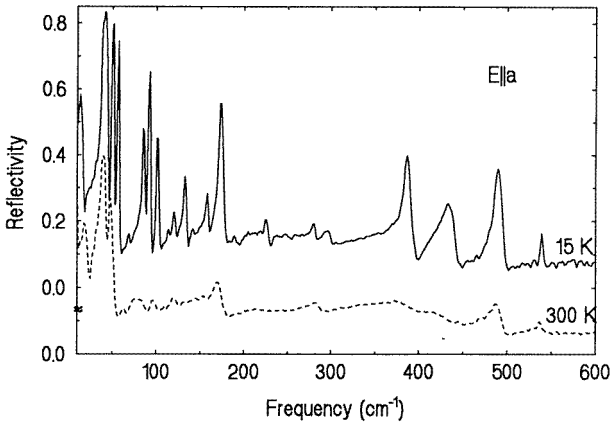

Figure 4. Infrared reflectivity spectra of LTT in the paraelectric phase at ambient pressure for the polarization $\boldsymbol{E}\|\boldsymbol{a}$.

103 cm^{-1} splits into two bands. According to the phase diagram in figure 2, at 50 K the FE phase exists above 240 MPa (see the new modes in figure 5 (top panel)). At 40 K and above 100 MPa the sample remains in the FE phase; therefore only a large pressure influence on the vibration modes is seen in figure 5 (bottom panel). This manifestation of the lowering of the crystal symmetry below T_c in FIR spectra is at variance with the published Raman data [11], where it was concluded that the crystal symmetry does not change below T_c. However, in [11] the PT temperature was not reached (see below). The crystal symmetry of the low-temperature FE phase is still unknown, but from the analogy of LTT with lithium ammonium tartrate monohydrate (LAT), which transforms near 100 K from $P2_12_12$ to a FE structure with the monoclinic space group $P12_11$ ($\boldsymbol{P}_s\|\boldsymbol{b}$), we may expect also a monoclinic symmetry of LTT in the FE phase. LTT is polar in the $\boldsymbol{a}$-direction; therefore this crystal should transform to the $P2_11$ space group. In the case of a monoclinic structure with $Z = 4$, the IR and Raman activity of all of the modes from the Brillouin zone centre should be as follows:

$$\Gamma_{LTT} = 113\mathrm{A}(\boldsymbol{a}, \boldsymbol{bc}, \boldsymbol{a}^2, \boldsymbol{b}^2, \boldsymbol{c}^2) + 112\mathrm{B}(\boldsymbol{b}, \boldsymbol{c}, \boldsymbol{ab}, \boldsymbol{ac}) + (\mathrm{A} + 2\mathrm{B})_{acoustic}. \tag{3}$$

The external modes of these are 35A + 34B. Accordingly, the number of IR-active ($\boldsymbol{E}\|\boldsymbol{a}$) modes below T_c should be roughly twice the number for $T > T_c$.

The SM is of B_3 symmetry in the paraelectric phase and it gives rise to the most intense band in the $\boldsymbol{cb}$ Raman spectra (see figure 6). Its frequency decreases at ambient pressure from 21 cm^{-1} (at 300 K) to $\sim$9 cm^{-1} (at T_c), i.e. it softens only incompletely because of the strong coupling with a transverse acoustic mode [10]. It has exactly the same temperature dependence as the SM already observed in FIR spectra [8, 9] with polarization $\boldsymbol{E}\|\boldsymbol{a}$. However, it is at variance with Raman results in [11], where this mode softens only down to 14.5 cm^{-1}. We assume that the sample in [11] was probably heated by the laser beam and the temperature T_c was not achieved. Under applied pressure, the SM frequency ν_s at constant temperature softens slowly to $\sim$9 cm^{-1} and above the critical pressure it increases more quickly (see figure 7). $\nu_s(T, p)$ obeys very well the formula

$$\nu_s(T, p) = \nu_0(T)\sqrt{p - p_{cr}(T)}$$

(see the broken curves in figure 7). No anomaly was observed near the temperature of the

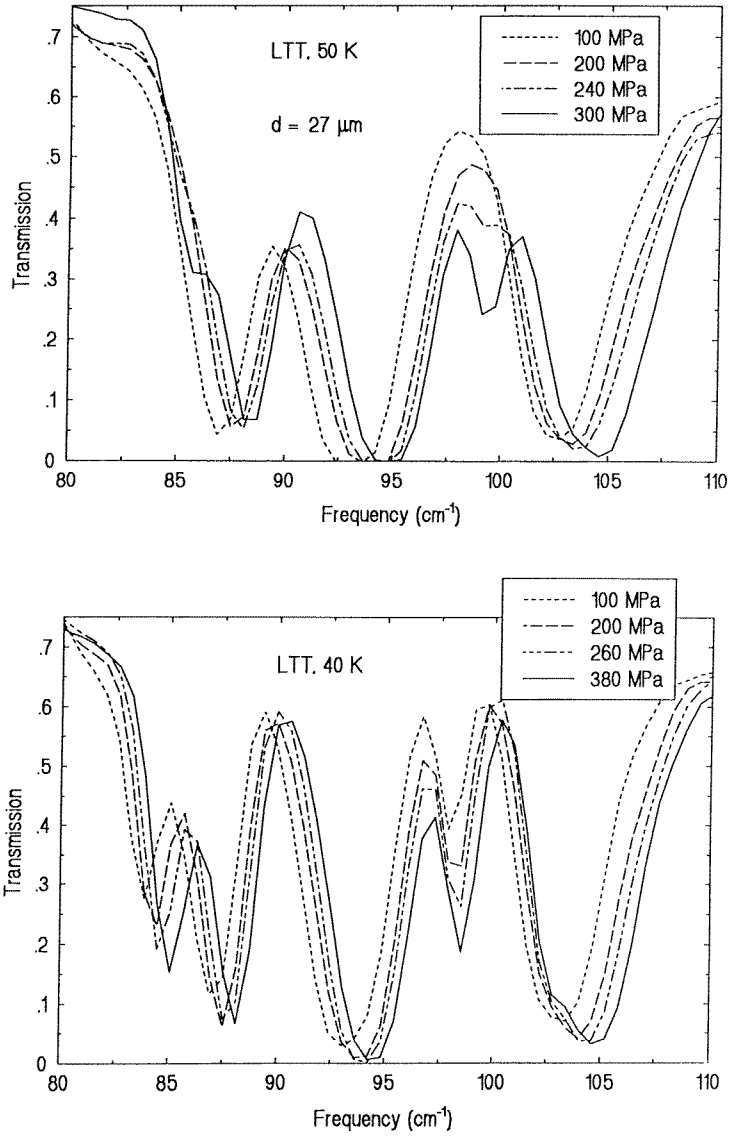

Figure 5. The pressure dependence of FIR transmission spectra for $\boldsymbol{E}\|\boldsymbol{a}$ at (top) 50 K (a paraelectric phase below 200 MPa) and (bottom) 40 K, where the sample is in the FE phase. The sample thickness $d = 27$ μm.

drop in ε'_a. This supports our point of view that the drop in ε'_a is not connected with a new PT but rather with a freezing of domain wall motion.

The SM is also revealed in our FIR spectra for the polarization $\boldsymbol{E}\|\boldsymbol{a}$ (figure 8). The temperature dependence of ν_s corresponds to our results from Raman measurements and to already published near-millimetre spectra in [9]. However, the SM frequency ν_s near T_c lies at the end of our spectral range, so a detailed evaluation of $\nu_s(T)$ is impossible. FIR spectra show that most other phonon modes are temperature and pressure independent. Only the mode near 90 cm^{-1} seems to be very sensitive to the temperature and pressure

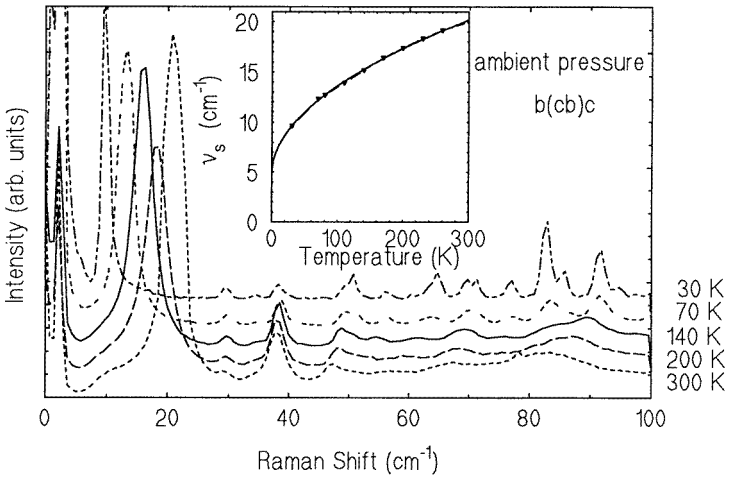

Figure 6. The temperature dependence of the Raman $\boldsymbol{b}(\boldsymbol{cb})\boldsymbol{c}$ spectra at ambient pressure. The softening of the lowest phonon is clearly seen. The inset shows the temperature dependence of the SM frequency fitted by the Cochran law.

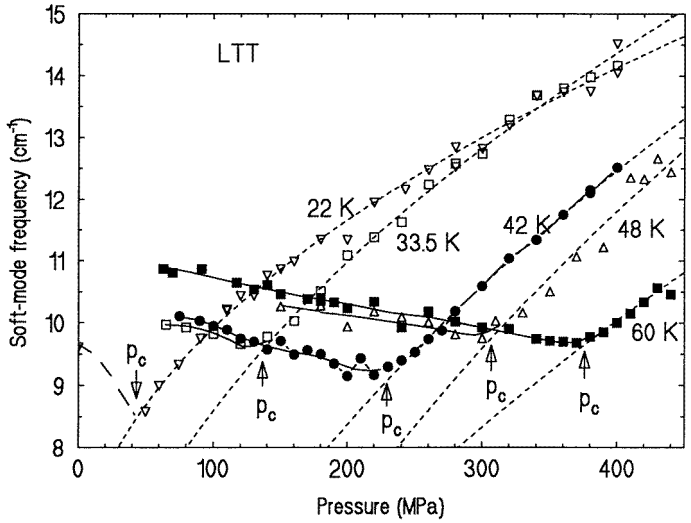

Figure 7. Pressure dependences of the soft-mode frequencies at different temperatures obtained from the Raman $\boldsymbol{b}(\boldsymbol{cb})\boldsymbol{c}$ spectra. The broken curves in the FE phase are results of the square-root fits.

changes and its frequency increases on cooling and/or on increasing pressure (see figures 4 and 7). In Rochelle salt [19], a similar large temperature and pressure dependence is shown by the mode at $\sim$80 cm^{-1}; therefore the two modes can probably be assigned to similar external vibrations.

From the minimum of $\nu_s(p)$ in figure 7 the critical temperature T_c and the critical pressure p_c can be evaluated. Pressure dependences of T_c obtained from dielectric and Raman experiments correspond within the experimental error (see figure 8). The nonlinear

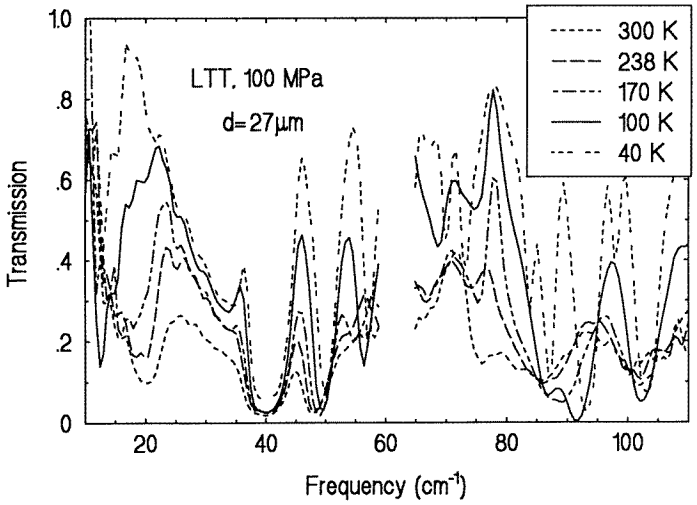

Figure 8. The temperature dependence of the FIR transmission spectra for the polarization $\boldsymbol{E}\|\boldsymbol{a}$ at 100 MPa. In the 59–65 cm^{-1} range, data are missing because of the opacity of the 50 μm thick beamsplitter (Mylar).

pressure dependence of T_c and T_{c2} obtained from dielectric measurement can be fitted with the formula $T_c(p) = T_c(0) + Ap^{1/2}$, where $T_c(0)$ = 11.6 K and $A = 6.89 \times 10^{-2}$ K $Pa^{-1/2}$ and 4.03×10^{-2} K $Pa^{-1/2}$ for T_c and T_{c2}, respectively.

From the Cochran law $\nu_s(T) = a\sqrt{T - T_0}$ for the SM frequency ν_s or from the Curie–Weiss law $\varepsilon_{cl}(T) = \varepsilon_\infty + C_w/(T - T_0)$ for the clamped permittivity ε_{cl} (at frequencies above the piezoelectric resonances), where C_w is the Curie–Weiss constant ($C_w = 1460$ K^{-1} for LTT), one can obtain the hypothetical PT temperature T_0 of the clamped system. Our Raman data at ambient pressure as well as submillimetre spectra give $T_0 = -60 \pm 5$ K for the LTT crystal. The real PT temperature $T_c = 11$ K is much higher due to piezoelectric coupling. The piezoelectric coupling parameter can be estimated according to the formula [20]

$$a_{14} = \sqrt{(T_c - T_0)c_{44}/\varepsilon_0 C_w}$$

where ε_0 is the permittivity of vacuum. Taking $c_{44} = 1 \times 10^{10}$ N m^{-2} from [7] we obtain $a_{14} = (7.4 \pm 1.9) \times 10^9$ N C^{-1}, which corresponds well to $a_{14} = 5.5 \times 10^9$ N C^{-1} in [7]. Hayashi *et al* [10] published $c_{44} = 2 \times 10^{10}$ N m^{-2} for which we get $a_{14} = (1.24 \pm 0.19) \times 10^{10}$ N C^{-1}.

Most FE and antiferroelectric (AFE) materials exhibit a linear pressure dependence of T_c. Several exceptions exist, like hydrogen-bonded FE and AFE of the KDP and ADP family, whose values of T_c decrease nonlinearly with pressure ($T_c \propto (p_c - p)^{0.5}$) and vanish at high pressure. Our square-root pressure dependence of T_c is a well known characteristic of quantum ferroelectricity [21]. The second one is the squared temperature dependence of the anomalous part of $1/\varepsilon'$ ($1/(\varepsilon' - \varepsilon_\infty) \propto (T - T_c)^2$) near p_c. This condition is very well fulfilled in our case 50–70 K above T_c at ambient pressure and even higher (see figure 9). Therefore one can expect large quantum fluctuations in LTT crystals near and below T_c.

Samara formulated an empirical rule (see [22, 23]) for *displacive* FE and AFE PT: in materials with a proper FE PT, where the PT is driven by a zone-centre polar transverse optic SM, T_c *decreases* with increasing pressure, whereas for an improper PT triggered by an optic SM with nonzero wavevector (in the case of an AFE PT the wavevector is

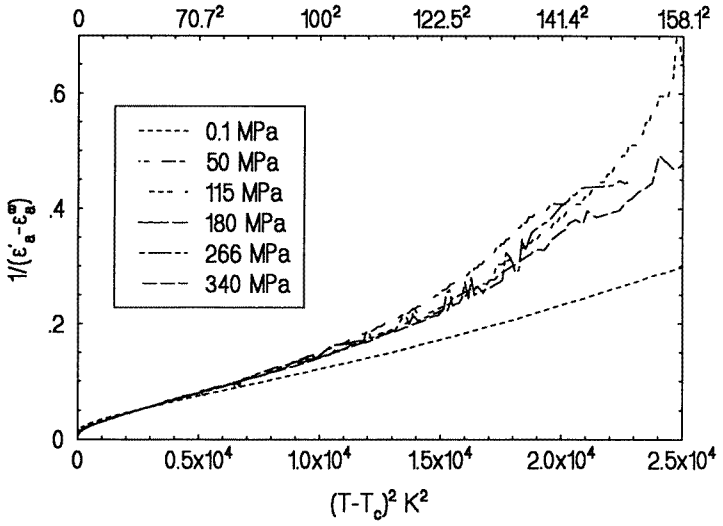

Figure 9. The reciprocal of $\varepsilon'_a - \varepsilon'^{\infty}_a$ versus the square of the temperature difference $T - T_c$ at different pressures.

from the Brillouin zone boundary) T_c *increases* with increasing pressure. However, several exceptions to this empirical rule exist, e.g. the behaviour of improper FE Co–I boracite ($Co_3B_7O_{13}I$) [24], the hydrogen-bonded pseudoproper FE $LiNH_4SO_4$ [25], AFE materials from the ADP family [23], and FE Rochelle salt (this hydrogen-bonded material displays, according to our recent investigations [19], a displacive PT). Peculiar behaviour is exhibited by $BaMnF_4$, which behaves according to Samara's rule up to 10 kbar whereupon the sign of dT_c/dp changes at higher pressures [26]. Also LTT, which belongs to the Rochelle salt family, does not obey Samara's empirical rule ($dT_c/dp > 0$ for LTT). It is interesting to note that all of the above-mentioned hydrogen-bonded ferroelectrics, which do not obey Samara's empirical rule, are characterized by a strong piezoelectric coupling between the optical SM and the acoustic mode.

In conclusion, we observed a strong increase of the FE PT temperature with hydrostatic pressure in LTT single crystals. A broad plateau in ε'_a below T_c was assigned to domain wall motions. The optical SM, which softens only incompletely due to its strong coupling with a transverse acoustic mode, was observed in IR as well as Raman spectra. On the basis of changes observed in our FIR spectra in the FE phase we propose it to have monoclinic symmetry ($P2_111$ space group). The are indications that LTT behaves as a quantum FE.

Acknowledgments

This work was supported by the Alexander-von-Humboldt Foundation and the Grant Agency of the Czech Republic (project No 202/95/1393).

References

[1] McCarthy G J, Schlegel L H and Sawaguchi E 1971 *J. Appl. Crystallogr.* **4** 180
[2] Kay M I 1978 *Ferroelectrics* **19** 159
[3] Matthias B T and Hulm J K 1951 *Phys. Rev.* **82** 108

[4] Fousek J, Cross L E and Seely K 1970 *Ferroelectrics* **1** 63
[5] Březina B, Janoušek V, Mareček V and Smutný F 1970 *Proc. European Mtg on Ferroelectricity* ed H E Müser and J Petersson (Stuttgart: Wissenschaftliche Verlagsgesellschaft) p 369
[6] Abe R, Kamiya N and Matsuda M 1974 *Ferroelectrics* **8** 557
[7] Sawaguchi E and Cross L E, 1971 *Ferroelectrics* **2** 37
[8] Gerbaux X, Hadni A, Pierron J and Messaadi S 1985 *Int. J. Infrared Millimetre Waves* **6** 131
[9] Volkov A A, Goncharov Yu G, Kozlov G V, Petzelt J, Fousek J and Březina B 1986 *Sov. Phys.–Solid State* **28** 1794
[10] Hayashi K, Deguchi K and Nakamura E 1992 *J. Phys. Soc. Japan* **61** 1357
[11] Khaller K E, Khaav A A, Novik V K and Gavrilova N D 1988 *Sov. Phys.–Solid State* **30** 47
[12] Busch G and Scherrer P 1935 *Naturwissenschaften* **23** 737
[13] Bornarel J, Fouskova A, Guyon P and Lajzerowicz J 1966 *Proc. Int. Mtg on Ferroelectricity (Prague)* vol II (Prague: Institute of Physics of the Czechoslovak Academy of Sciences) pp 81–90
[14] Sidorkin A S, Burdanina N A and Kamysheva L N 1984 *Sov. Phys.–Solid State* **26** 1910
[15] Baski A A, Oliver W F and Scott J F 1987 *Ferroelectrics Lett.* **7** 171
[16] Dugdale J S and Franck J P 1964 *Phil. Trans. R. Soc.* **1** 257
[17] Latush L T, Rabkin L M, Torgashev V I, Yuzyuk Yu I, Shuvalov L A and Schagina N M 1987 *Ferroelectrics* **75** 455
[18] Bhattacharjee R, Jain Y S, Raghubanshi G and Bist H D 1988 *J. Raman Spectrosc.* **19** 51
[19] Kamba S, Schaack G and Petzelt J 1995 *Phys. Rev.* B **51** 14 998
[20] Petzelt J, Goncharov Yu G, Kozlov G V, Volkov A A, Wyncke B and Brehat F 1984 *Czech. J. Phys.* B **34** 887
[21] Höchli U T 1981 *Ferroelectrics* **35** 17
[22] Samara G A, Sakudo T and Yoshimitsu K 1975 *Phys. Rev. Lett.* **36** 1767
[23] Samara G A and Peercy P S 1981 *Solid State Physics, Advances in Research and Applications* vol 36, ed H Ehrenreich, F Seitz and D Turnbull (New York: Academic) p 1
[24] Fousek J, Smutný F, Frenzel C and Hegenbarth E 1972 *Ferroelectrics* **4** 23
[25] Torgashev V I, Dvořák V and Smutný F 1984 *Phys. Status Solidi* **126** 459
[26] Samara G A and Richards P M 1976 *Phys. Rev.* B **14** 5073